Thin Solid Films 517 (2009) 1874–1879

Contents lists available at ScienceDirect

Thin Solid Films

journal homepage: www.elsevier.com/locate/tsf

Atomic layer deposition of iron(III) oxide on zirconia nanoparticles in a fluidized bed reactor using ferrocene and oxygen

Jonathan R. Scheffe [a], Andrea Francés [a,c], David M. King [a], Xinhua Liang [a], Brittany A. Branch [a], Andrew S. Cavanagh [a,b], Steven M. George [a,b], Alan W. Weimer [a,*]

[a] Department of Chemical and Biological Engineering, University of Colorado, Boulder, CO 80309, USA
[b] Department of Chemistry and Biochemistry, University of Colorado, Boulder, CO 80309, USA
[c] Department of Chemical Engineering, Tecnológico de Monterrey, Mexico

ARTICLE INFO

Article history:
Received 29 July 2008
Received in revised form 18 September 2008
Accepted 22 September 2008
Available online 30 September 2008

Keywords:
Atomic layer deposition (ALD)
Iron oxide
Ferrocene
Nanoparticles
Thin film

ABSTRACT

Conformal films of amorphous iron(III) oxide and α-Fe_2O_3 have been coated on zirconia nanoparticles (26 nm) in a fluidized bed reactor by atomic layer deposition. Ferrocene and oxygen were alternately dosed into the reactor at temperatures between 367 °C and 534 °C. Self-limiting chemistry was observed via *in situ* mass spectrometry, and by means of induced coupled plasma-atomic emission spectroscopy analysis. Film conformality and uniformity were verified by high resolution transmission electron microscopy, and the growth rate was determined to be 0.15 Å per cycle. Energy dispersive spectroscopy, X-ray diffractometry, and X-ray photoelectron spectroscopy were utilized as a means to determine film composition at each deposition temperature. Over all of the deposition temperatures investigated, films were deposited as amorphous iron(III) oxide. However, after heat treatment at 850 °C in air and N_2 atmospheres, α-Fe_2O_3 was the predominant species.

1. Introduction

Iron(III) oxide thin films have received significant attention in recent years due to their potential for use in catalytic, optical, electrical and magnetic applications. Iron oxide based Fisher–Tropsch synthesis catalysts, along with cobalt oxide based catalysts, are used industrially to convert synthesis gas to liquids with low H_2/CO ratios and have low CH_4 selectivities [1,2]. Fe_2O_3 is used extensively to catalyze the dehydrogenation of ethylbenzene for styrene synthesis due to the intermediate adsorption strength of Fe^{3+} for ethylbenzene and styrene [3–6]. Iron(III) oxide has a high propensity to transmit visible light while absorbing light in the infrared range, and as such can be used as a solar filter on windows to reduce radiative heat transfer [7,8]. The band gap of iron (III) oxide is 2.0 eV, which allows for the capability of absorbing 38% of the solar spectrum. Relative to TiO_2, which typically only absorbs the ultraviolet portion of the solar spectrum (~5%) it is well suited to help improve the efficiency of photoelectrochemical hydrogen production [9,10]. Additionally, there has been recent extensive research involving iron oxide nanoparticle synthesis, as the nanosized features exhibit different properties than the bulk material and have been used for several important magnetic applications [11–13]. The properties of iron (III) oxide thin films are highly dependent on thickness, morphology and chemical composition, and therefore it is advantageous to have precise control of these properties.

Currently, there are several methods employed for iron oxide thin film deposition, including chemical vapor deposition (CVD), sputtering, arc-plasma spray deposition, and various wet chemistry methods such as sol–gel deposition [7,13–17]. However, there are disadvantages to these methods that limit their ability to precisely control film thickness, morphology and chemical composition. For example, sol–gel methods have the capability to deposit films as thin as 100 nm, but it can be difficult to control its chemical state, and many times films are not uniform and conformal [16–18]. Sputtering is able to deposit thinner films than those of wet chemistry methods, however due to the continuous bombardment of highly energetic species onto the film, the equilibrium state of the deposited oxide is very difficult to control [15,16]. Perhaps the most common technique for iron oxide thin film deposition is CVD. This process involves vapor phase precursors reacting within a deposition chamber on a substrate surface, and as a result there are no geometrical limitations [19]. However, film thickness is difficult to control because this process is not self-limiting, resulting in films that are generally micron-sized or thicker [20]. Films are typically non-conformal and granular due to the fact that excess vapor phase reactants may nucleate and precipitate on the substrate surface. Additionally, film stoichiometry is difficult to control, as the amount of precursor delivered into the deposition chamber is dependent on its vapor pressure [21].

---

[*] Corresponding author. University of Colorado, Boulder, Department of Chemical and Biological Engineering, 1111 Engineering Dr., Boulder, CO 80309-0424, USA. Tel.: +1 303 492 3759; fax: +1 303 492 4341.
E-mail address: Alan.Weimer@Colorado.edu (A.W. Weimer).

0040-6090/$ – see front matter © 2008 Elsevier B.V. All rights reserved.
doi:10.1016/j.tsf.2008.09.086

Atomic layer deposition (ALD) is a self-limiting technique that is capable of depositing highly conformal films one molecular layer at a time [22–25]. Deposition is based upon the principle of splitting a binary reaction (typical of CVD) into two half-reactions and alternating the exposure of gas phase precursors of each half-reaction to a surface, as shown below:

$$\text{Binary reaction}: x\cdot \mathrm{M(L)}_n + y\cdot \mathrm{H_2O} \rightarrow \mathrm{M}_x\mathrm{O}_y + n\cdot \mathrm{(HL)}$$

$$\text{Half}-\text{reaction1}: [\mathrm{S}]:(\mathrm{OH})_y^* + x(\mathrm{ML}_n) \rightarrow [\mathrm{S}]:\mathrm{O}_y\mathrm{M}_x(\mathrm{L})_{n-y}^* + y(\mathrm{HL})$$

$$\text{Half}-\text{reaction2}: [\mathrm{S}]:\mathrm{O}_y\mathrm{M}_x(\mathrm{L})_{n-y}^* + y\mathrm{H_2O} \rightarrow [\mathrm{S}]:\mathrm{M}_x\mathrm{O}_y:(\mathrm{OH})_y^* + n{-}y(\mathrm{HL}),$$

where M represents the metal species, n is the number of ligands (L), x:y is the metal to oxide ratio, [S] represents a surface site, and * represents an active surface species [26]. Operating conditions are controlled in such a way that the precursors of one half-reaction react only with the precursors of the other. This ensures atomic level control, since there is at most one sub-monolayer of added species per half-reaction [27].

Iron oxide ALD has been demonstrated on a wide array of crystalline surfaces using $\mathrm{Fe(thd)_3}$ and $\mathrm{Fe(acac)_3}$ as precursors [28,29]. Recently, $\mathrm{Fe(C_5H_5)_2}$ (ferrocene) and oxygen have been used to deposit iron oxide films onto Si(100) and anodic aluminum [30]. The growth rates on Si (100) and anodic aluminum were 0.14 nm and 0.06 nm per cycle, respectively. At deposition temperatures below 500 °C a mixture of hematite and an unidentified phase was present. In this work, ALD of iron oxide on zirconia nanoparticles using ferrocene and oxygen is investigated. Films are deposited in a fluidized bed reactor (FBR) at temperatures ranging from 367 °C to 534 °C. They are shown to be highly conformal and uniform and can be controlled with angstrom level precision. As-deposited, the films are amorphous iron(III) oxide, but with heat treatment can be crystallized into α-$\mathrm{Fe_2O_3}$.

2. Experimental details

2.1. Material preparation

A schematic representation of the FBR is shown in Fig. 1. The reactor is 3.5 cm in diameter and includes a porous stainless steel (SS) distributor plate and filter at the inlet and outlet, respectively. These are used to prevent particles from leaving the reactor, while allowing gas to pass through freely. The details of this reactor configuration have been described elsewhere [26]. Product gases were measured using a Stanford Research Systems QMS series mass spectrometer.

Fluidization was accomplished at reduced pressure in conjunction with a mechanical vibration platform, as shown in Fig. 1. Mechanical vibration has been shown to aid in overcoming interparticle forces present between nanoparticles, resulting in smaller aggregate sizes and a decreased minimum fluidization velocity [30]. The pressure drop across the bed was measured as a function of gas flow rate in order to maintain fluidization throughout the ALD cycle.

The ALD cycle consisted of dosing ferrocene (99% purity acquired from Alfa Aesar®) and high purity oxygen (99.9%) in alternate doses into the reactor at temperatures ranging from 367 °C to 534 °C. Ferrocene was delivered into the reactor using a 200 cc bubbler (Precision Fabricators Ltd.) heated to 60 °C and nitrogen was employed as a carrier gas. The reactor was then purged with nitrogen in order to remove any excess ferrocene and by-products. Once purged, oxygen was dosed, followed by another nitrogen purge. All lines were heated to 65 °C in order to prevent any ferrocene vapor from depositing. A three factor central composite experimental design, shown in Fig. 2, was carried out with temperature, ferrocene dosing time, and oxygen dosing time all varying accordingly.

2.2. Material characterization

Visual inspection of the films was carried out using a 200 kV JEOL 2010F Schottky field emission high resolution transmission electron microscope (HRTEM). Film composition was determined via energy dispersive spectroscopy (EDS), X-ray diffraction (XRD, Scintag PAD5 Powder Diffractometer, CuKα radiation, $\lambda = 1.5406$ Å), and X-ray photoelectron spectroscopy (XPS, PHI 5600, Physical Electronics Inc., Al Kα). EDS results were obtained from a spectrometer that was coupled with the Schottky field emission TEM. XRD analysis was performed using a scan rate of 2°/min and step size of 0.2°. A pass energy of 58.7 eV and step size of 0.2 eV were used during XPS analysis. The resulting scans were internally calibrated by shifting the C 1s peak to 285.0 eV. Induced coupled plasma-atomic emission

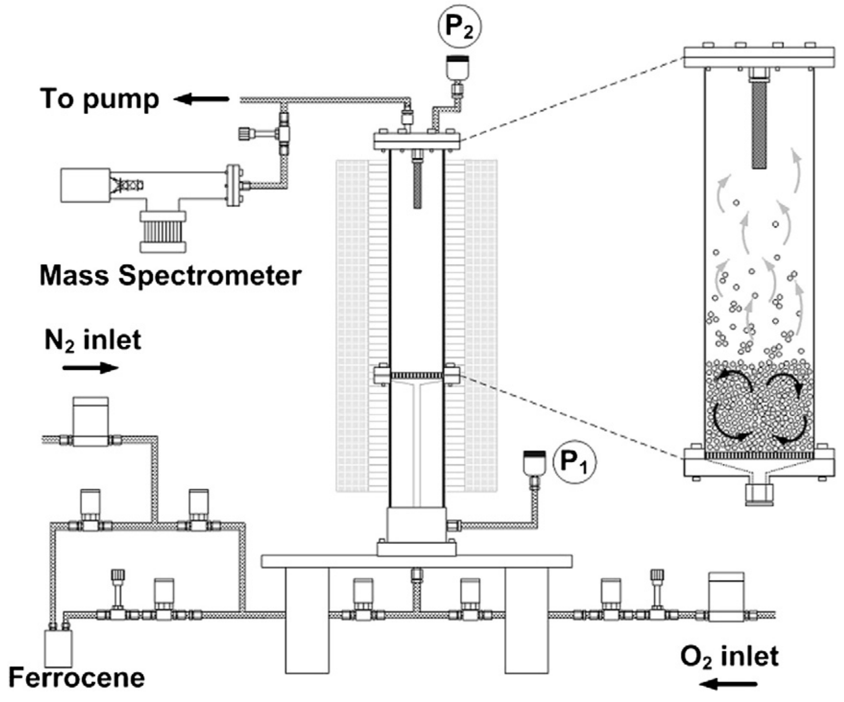

Fig. 1. Schematic diagram of the ALD fluidized bed reactor.